



Transfer reactions of exotic nuclei including core deformations: ^{11}Be and ^{17}C P. Punta ^{*}*Departamento de FAMN, Facultad de Física, Universidad de Sevilla, Apartado 1065, E-41080 Sevilla, Spain*J. A. Lay [†] and A. M. Moro [‡]*Departamento de FAMN, Facultad de Física, Universidad de Sevilla, Apartado 1065, E-41080 Sevilla, Spain
and Instituto Interuniversitario Carlos I de Física Teórica y Computacional (iCI), Apartado 1065, E-41080 Sevilla, Spain*

(Received 19 May 2023; accepted 28 July 2023; published 28 August 2023)

Background: Reactions with halo nuclei from deformed regions exhibit important deviations from the inert core + valence picture. Structure and reaction formalisms have recently been extended or adapted to explore the possibility of exciting the underlying core.

Purpose: We will study up to what extent transfer reactions involving halo nuclei ^{11}Be and ^{17}C can be reproduced with two different models that have previously shown a good success reproducing the role of the core in light halo nuclei.

Methods: We focus on the structure of ^{11}Be and ^{17}C with two core + valence models: Nilsson and a semimicroscopic particle-rotor model using antisymmetrized molecular dynamic calculations of the cores. These models are later used to study $^{16}\text{C}(d, p)^{17}\text{C}$ and $^{11}\text{Be}(p, d)^{10}\text{Be}$ transfer reactions within the adiabatic distorted wave approximation. Results are compared with three different experimental data sets.

Results: A good reproduction of both the structure and transfer reactions of ^{11}Be and ^{17}C is found. The Nilsson model provides an overall better agreement for the spectrum and reactions involving ^{17}C while the semimicroscopic model is more adequate for ^{11}Be , as expected, since the ^{17}C core is closer to an ideal rotor.

Conclusions: Both models show promising results for the study of transfer reactions with halo nuclei. We expect that including microscopic information in the Nilsson model, following the spirit of the semimicroscopic model, can provide a useful, yet simple framework for studying newly discovered halo nuclei.

DOI: [10.1103/PhysRevC.108.024613](https://doi.org/10.1103/PhysRevC.108.024613)**I. INTRODUCTION**

The study of exotic nuclei is one of the main topics in current nuclear physics research. They are nuclei far from the stability line, with a rather different ratio of protons to neutrons from that of stable nuclei. Because of that, they usually exhibit very different properties from those of stable nuclei. A particularly interesting case is that of halo nuclei. These are weakly bound systems composed of one or two highly delocalized valence particle(s) and a relatively compact core. As a schematic picture, the valence particles form a *halo* of matter around the core.

Weakly bound nuclei are conveniently described within few-body models, in which deformations of the fragments are usually ignored. However, *core deformations* are known to affect significantly both the structure and the dynamics of these systems [1–4]. Therefore, deformation needs to be included in structure and reaction models, for a meaningful and reliable description of reactions including these nuclei.

In previous works, the effect of core deformations in nuclear reactions has been included within the particle-rotor model, which is based on a weak-coupling limit. This model may be inaccurate for well-deformed nuclei, for which approaches based on the strong-coupling limit, such as the well-known Nilsson model, might provide a more suitable framework.

In this work, we present an exploratory study of the deformed weakly bound nuclei ^{17}C and ^{11}Be within the Nilsson model. A two-body model is considered: a neutron moving in a deformed potential generated by the core. Although this is not the first application of the Nilsson model to these nuclei [5,6], a novelty of our work is the use of a pseudostate method to compute the bound and unbound states of the system. In this method, the energies of these states and their associated wave functions are obtained diagonalizing the internal Hamiltonian in a basis of square-integrable functions, for which we employ the transformed harmonic-oscillator functions (THO) which has been successfully applied to the discretization of the continuum of weakly bound nuclei for its application to breakup and transfer direct reactions both for two-body and three-body systems [2,7].

For comparison purposes, we also present calculations for the same nuclei based on the so-called PAMD model, in which the Hamiltonian is constructed using the transition densities

^{*}ppunta@us.es[†]lay@us.es[‡]moro@us.es

of the corresponding cores calculated in the antisymmetrized molecular dynamics (AMD) formalism. The PAMD model was introduced in Ref. [8] and applied to ^{11}Be and ^{19}C with a promising reproduction of the structure of both nuclei. Results for ^{17}C can be found in Refs. [9,10].

To assess the quality and reliability of the developed models, the calculated wave functions are applied to transfer reactions involving these nuclei. Two transfer reactions have been studied by implementing the results of the structure calculations, $^{16}\text{C}(d, p)^{17}\text{C}$ and $^{11}\text{Be}(p, d)^{10}\text{Be}$. The adiabatic distorted-wave approximation (ADWA) [11] has been used for this purpose. The results of theoretical calculations are compared with the experimental data recently measured in GANIL and RCNP.

The Nilsson scheme has been previously applied to reactions involving light exotic nuclei [12–14] but only to extract the required spectroscopic factors, which are then combined with single-particle wave functions calculated in a spherical potential. However, to the best of our knowledge, this is the first time that the effect of the deformation is considered also on the radial form factor of the transfer reaction for exotic nuclei and, not only, for the calculation of the corresponding spectroscopic factor. As already shown in stable nuclei [15], there is a non-negligible effect on the radial extension of the form factor due to the deformation. One can only expect this effect to increase considerably in the case of halo nuclei.

The paper is organized as follows: Sec. II is about the structure formalism, it focuses on the description of the novel approach based on the Nilsson model and also briefly explains the PAMD model. Section III shows the application of the ADWA approach to one neutron transfer reactions. The results of the application of the two models to the ^{17}C and ^{11}Be nuclei can be seen in Sec. IV. In Sec. V we study the reactions $^{16}\text{C}(d, p)^{17}\text{C}$ and $^{11}\text{Be}(p, d)^{10}\text{Be}$. Finally, we discuss the main results in Sec. VI.

II. STRUCTURE FORMALISM

We consider a composite nucleus, described as a two-body system, comprising a weakly bound nucleon coupled to a core. The Hamiltonian of the system can be written as

$$\mathcal{H} = T(\vec{r}) + V_{\ell s}(r)(\vec{\ell} \cdot \vec{s}) + V_{vc}(\vec{r}, \xi) + h_{\text{core}}(\xi), \quad (1)$$

where $T(\vec{r})$ is the kinetic energy operator for the relative motion between the valence and the core, $h_{\text{core}}(\xi)$ is the Hamiltonian of the core, and $V_{vc}(\vec{r}, \xi)$ is the effective valence-core interaction. A spin-orbit term with the usual radial dependence $V_{\ell s}(r)$ is added to this valence-core interaction. ξ denotes the core degrees of freedom, so the dependence of $V_{vc}(\vec{r}, \xi)$ on it accounts for core-excitation effects.

In this work, two different models have been considered, which can be regarded as opposite limits of the coupling strength, namely, strong and weak coupling. For the strong coupling, the Nilsson model, as formulated in Ref. [16], was used. For the weak-coupling case, we employ the semimicroscopic particle-plus-AMD (PAMD) model proposed in Ref. [8]. This second model obtains the coupling potential $V_{vc}(\vec{r}, \xi)$ convoluting an effective NN interaction with

microscopic transition densities of the core nucleus calculated with antisymmetrized molecular dynamics (AMD) [17,18].

The eigenfunctions of the Hamiltonian, for a given energy ε , are characterized by the parity π and the total angular momentum \vec{J} , resulting from the coupling of the angular momentum \vec{j} of the valence particle to the core angular momentum \vec{I} . These functions can be generically expressed as

$$\Psi_{\varepsilon M}^{J^\pi}(\vec{r}, \xi) = \sum_{\alpha} R_{\varepsilon \alpha}^{J^\pi}(r) \Phi_{\alpha J}^M(\hat{r}, \xi), \quad (2)$$

where $\Phi_{\alpha J}^M(\hat{r}, \xi)$ refers to the eigenstates of J^2 and J_z resulting for the coupling of \vec{j} to \vec{I} ,

$$\Phi_{\alpha J}^M(\hat{r}, \xi) \equiv [\mathcal{Y}_{\ell s}^j(\hat{r}) \otimes \phi_I(\xi)]_{JM}. \quad (3)$$

Here, $\vec{\ell}$ is the orbital angular momentum of the valence particle relative to the core, which couples to the spin of the valence particle \vec{s} to give the particle total angular momentum \vec{j} . The label α denotes the set of quantum numbers $\{\ell, s, j, I\}$. $\mathcal{Y}_{\ell s}^{jm}(\hat{r})$ denotes the wave function resulting from coupling the spin of the valence particle with the corresponding spherical harmonic.

A. Nilsson model

A key aspect of the Nilsson model is that, instead of considering the relative motion valence-core in the space fixed laboratory frame (\vec{r}), it considers the intrinsic frame (\vec{r}'), which rotates jointly with the core. For this frame, if we assume that the core has a permanent deformation, we can assume that the potential V_{vc} depends on \vec{r}' with the same geometry and does not depend explicitly on ξ .

In the original Nilsson model, the valence-core interaction is assumed to be an anisotropic harmonic-oscillator potential. However, in this work, a more realistic Woods-Saxon potential is used and a permanent axially symmetric quadrupole deformation is applied. Following [16], we obtain to first order in the deformation parameter β :

$$V_{vc}^{\text{Nilsson}}(r, \theta') = V_c(r) - \beta r \frac{dV_c(r)}{dr} Y_{20}(\theta'), \quad (4)$$

where θ' is the angle with respect to the symmetry axis of the core and r' coincides with r , the relative distance between core and valence. Note that deformations with $\beta > 0$ and $\beta < 0$ correspond, respectively, to prolate and oblate shapes. Expression (4) can be in principle applied to deform any central potential $V_c(r)$, and, in particular, if an isotropic harmonic-oscillator potential is used, the original Nilsson model term for the anisotropic oscillator is recovered.

Considering this potential and the kinetic and spin-orbit terms, with the parameters from [5] for ^{17}C and different values of β , the Nilsson diagram shown in Fig. 1 is obtained. This diagram shows how the single-particle energy levels of the valence nucleon change as the deformation parameter varies. Except for $\beta = 0$, these levels do not have well-defined values of ℓ and j , but they can be characterized by their parity π and the projection Ω of \vec{j} along the axial symmetry axis. With the deformation, the spherical levels degenerated in Ω separate according to their Ω values and begin to mix with other levels

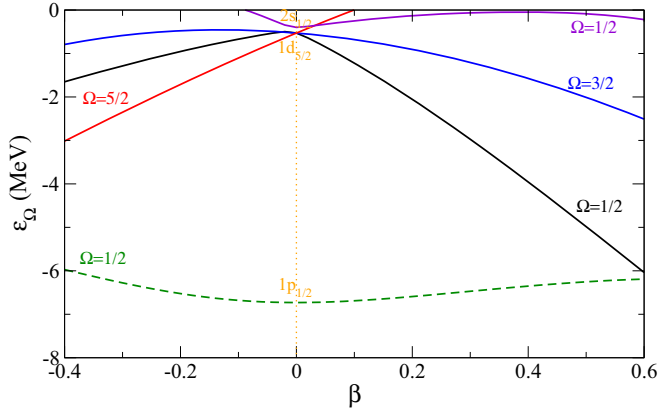


FIG. 1. Nilsson diagram obtained for ^{17}C by diagonalization in the THO basis using the parameters from [5]. Solid lines represent positive-parity levels, while negative-parity levels are represented by dashed lines.

with the same Ω . For $\beta > 0$, the Nilsson levels originating from the same spherical level split in energy according to their Ω value, with higher Ω values lying at higher energies. Due to the symmetry of the system, the Ω and $-\Omega$ projection states are equivalent, therefore each Nilsson level has twofold degeneracy.

The complete Hamiltonian of the system also includes an intrinsic core term. In this case, the core is approximated by a perfect rotor. Therefore, h_{core} depends on the angular momentum of the core, but the relation $\vec{I} = \vec{J} - \vec{j}$ can be used, resulting in

$$h_{\text{core}}^{\text{Nilsson}} = \frac{\hbar^2}{2\mathcal{J}} \vec{I}^2 = \frac{\hbar^2}{2\mathcal{J}} (\vec{J} - \vec{j})^2, \quad (5)$$

where \mathcal{J} is the moment of inertia of the core. This collective term mixes the different single-particle Nilsson levels, causing Ω to stop being a good quantum number for the eigenstates of the full Hamiltonian.

In this model, the eigenstates are expressed as

$$\Psi_{\varepsilon M}^{J\pi}(\vec{r}', \omega) = \sum_{\nu} R_{\varepsilon\nu}^{J\pi}(r) \Phi_{\nu J}^M(\hat{r}', \omega), \quad (6)$$

where now ν corresponds to the quantum numbers $\{\ell, s, j, \Omega\}$ with $\Omega > 0$. The functions $\Phi_{\nu J}^M(\hat{r}', \omega)$ are defined as

$$\begin{aligned} \Phi_{\nu J}^M(\hat{r}', \omega) &= \frac{\sqrt{2J+1}}{4\pi} [\mathcal{Y}_{\ell s}^{j\Omega}(\hat{r}') \mathcal{D}_{M\Omega}^J(\omega)^* \\ &+ (-1)^{J-j} \mathcal{Y}_{\ell s}^{j-\Omega}(\hat{r}') \mathcal{D}_{M-\Omega}^J(\omega)^*]. \end{aligned} \quad (7)$$

The definition of Ref. [19] is used for the rotation matrices $\mathcal{D}_{M\Omega}^J(\omega)$ and the three Euler angles are denoted by ω . The functions $\Phi_{\nu J}^M(\hat{r}', \omega)$ are orthonormal and take into account the symmetry regarding the Ω and $-\Omega$ projections.

Assuming the core to be a rotor, expressions (2) and (6) are equivalent and can be interchanged using the relation

$$R_{\varepsilon\alpha}^{J\pi}(r) = \sqrt{\frac{2I+1}{2J+1}} \sqrt{1+(-1)^J} \sum_{\Omega} \langle j\Omega I 0 | J\Omega \rangle R_{\varepsilon\nu}^{J\pi}(r), \quad (8)$$

where ℓ and j are the same for α and ν and $\langle j\Omega I 0 | J\Omega \rangle$ is a Clebsch-Gordan coefficient. This expression is obtained by transforming $\Phi_{\varepsilon\alpha}^M(\vec{r}, \xi)$ into $\Phi_{\varepsilon\nu}^M(\hat{r}', \omega)$, using the properties of the rotational matrices.

B. The transformed harmonic oscillator basis

In this section, we briefly review the method followed in the present work to obtain the eigenvalues of the Hamiltonian and their associated wave functions.

The eigenstates of a two-body Hamiltonian, like that of Eq. (1), follow the expression (2) or (6), and the radial functions $R_{\varepsilon\alpha}^{J\pi}(r)$ or $R_{\varepsilon\nu}^{J\pi}(r)$ can be determined in several ways. A common procedure is to insert the expansion (2) into the Schrödinger equation, giving rise to a set of coupled differential equations for the radial functions $R_{\varepsilon\alpha}^{J\pi}(r)$ (see, e.g., Ref. [20]).

Alternatively, these functions can be obtained by diagonalizing the Hamiltonian in a discrete basis. This basis is chosen in the form $\psi_{n\tau JM}^{\text{basis}} = R_{n\ell}^{\text{basis}}(r) \Phi_{\tau J}^M$, where τ can be $\alpha = \{\ell, s, j, I\}$ or $\nu = \{\ell, s, j, \Omega\}$ and the function $\Phi_{\tau J}^M$ is given by (3) or (7), respectively. Thus, the eigenstates of the Hamiltonian can be expanded in the discrete basis as

$$\Psi_{iM}^{J\pi} = \sum_{n\tau} C_{n\tau}^{iJ\pi} \psi_{n\tau JM}^{\text{basis}} = \sum_{n\tau} C_{n\tau}^{iJ\pi} R_{n\ell}^{\text{basis}}(r) \Phi_{\tau J}^M. \quad (9)$$

There are many possible choices for the basis functions $R_{n\ell}^{\text{basis}}(r)$ (Gaussian, harmonic oscillator, Laguerre, etc.). In this work we use the transformed harmonic-oscillator (THO) basis, obtained from the harmonic-oscillator basis with an appropriate local scale transformation (LST) [21,22].

If the LST function is denoted by $s(r)$, the THO states are obtained as

$$R_{n\ell}^{\text{THO}}(r) = \frac{s}{r} \sqrt{\frac{ds}{dr}} R_{n\ell}^{\text{HO}}[s(r)], \quad (10)$$

where $R_{n\ell}^{\text{HO}}(s)$ (with $n = 1, 2, \dots$) is the radial part of the usual HO functions. According to the definition given above, the LST is indeed not unique. Here, we adopted a parametric form for the LST from Karataglidis *et al.* [23]:

$$s(r) = \left[\frac{1}{\left(\frac{1}{r}\right)^m + \left(\frac{1}{\gamma\sqrt{r}}\right)^m} \right]^{\frac{1}{m}}, \quad (11)$$

which depends on the parameters m and γ . The extension of $R_{n\ell}^{\text{HO}}(s)$ will also depend on the oscillator length b . Note that, asymptotically, the function $s(r)$ behaves as $s(r) \sim \gamma\sqrt{r}$ and hence the functions obtained by applying this LST to the HO basis behave at large distances as $\exp(-\gamma^2 r/2b^2)$. Therefore, the ratio γ/b can be related to an effective linear momentum, $k_{\text{eff}} = \gamma^2/2b^2$, which governs the asymptotic behavior of the THO functions. As the ratio γ/b increases, the radial extension of the basis decreases and, consequently, the eigenvalues obtained upon diagonalization of the Hamiltonian in the THO basis tend to spread at higher excitation energies. Therefore, γ/b determines the density of eigenstates as a function of the excitation energy. In all calculations presented in this work, the power m has been taken as $m = 4$. This choice is

discussed in Ref. [23] where the authors found that the results are weakly dependent on m .

Note that, by construction, the family of functions $R_{n\ell}^{\text{THO}}(r)$ constitute a complete orthonormal set. Moreover, they decay exponentially at large distances, thus ensuring the correct asymptotic behavior for the bound wave functions. In practical calculations, a finite set of τ channels and wave functions as in Eq. (10) are retained, and the Hamiltonian is diagonalized in this truncated basis, giving rise to a set of eigenvalues $\{\varepsilon_i^{J^\pi}\}$ and their associated eigenfunctions, $\{\Psi_{iM}^{J^\pi}\}$. As the basis size is increased, the eigenstates with negative energy will tend to the exact bound states of the system, while those with positive eigenvalues can be regarded as a finite representation of the unbound states.

This analytical THO basis has been successfully applied to the structure and reactions of two-body systems in Ref. [24] and generalized to the case in which core excitations are included [25].

III. ONE-NEUTRON TRANSFER REACTIONS

As in the case of stable nuclei, a significant source of information of halo nuclei stems from the analysis of transfer reactions involving these nuclei. We focus on $C(d, p)A$ and $A(p, d)C$ reactions, where A corresponds to one of the nuclei studied with our models and C to its respective core. In this case, they are studied using the adiabatic distorted-wave approximation (ADWA) [11]. The formalism for this approximation is identical to that of the distorted-wave Born approximation (DWBA), with the difference that adiabatic potentials are calculated between deuteron and the other nucleus. The reason for using ADWA instead of DWBA is to take into account, approximately, the effect of deuteron break-up on the calculation.

Considering for definiteness the (d, p) case, the transition amplitudes are calculated in *post* form:

$$\mathcal{T}_{if}^{\text{post}} = \langle \chi_{\vec{k}_{pA}}^{(-)} \psi_{CA} | V_{pn} + U_{pC} - U_{pA} | \chi_{\vec{k}_{dC}}^{(+)} \psi_d \rangle, \quad (12)$$

where $\chi_{\vec{k}_{dC}}$ and $\chi_{\vec{k}_{pA}}$ are distorted waves for the entrance and exit channels, respectively, depending on the corresponding deuteron and proton momenta. The function ψ_d stands for deuteron ground-state wave function, generated with the potential V_{pn} . The operators U_{pC} and U_{pA} are optical potentials for the $p + C$ and $p + A$ systems. Our structure model is implemented in the overlap $\psi_{CA} \equiv \langle C|A \rangle$. Starting from expression (2), it can be shown

$$\psi_{CA}(\vec{r}) = \sum_j \langle JM | j m_j I m_I \rangle R_{\varepsilon\alpha}^{J^\pi}(r) \mathcal{Y}_{\ell s}^j(\hat{r}). \quad (13)$$

Therefore, only the $R_{\varepsilon\alpha}^{J^\pi}(r)$ functions resulting from our models are needed. The transition amplitudes are calculated for given states of nuclei A and C , in our models, which implies well-defined $\{J^\pi, \varepsilon, I\}$ values with their compatible j values.

Similarly, in the (p, d) case, the transition amplitudes are calculated in *prior* form. The amplitudes and their corresponding cross sections are calculated by using the FRESKO code [26].

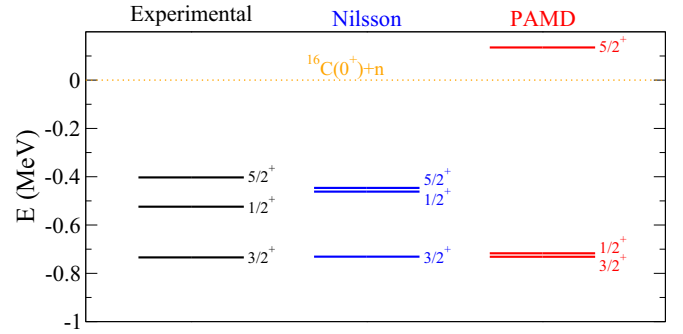


FIG. 2. Experimental and calculated energy levels of ^{17}C . Starting from the left, the second column is the Nilsson model and the third is the PAMD. Experimental values are from Refs. [29,30].

IV. APPLICATION TO ^{17}C AND ^{11}Be

The Nilsson Hamiltonian has been built and diagonalized in the THO basis for the ^{17}C and ^{11}Be systems. To ensure convergence, the values $0 \leq \ell \leq 6$ and $1 \leq n \leq 30$ have been considered. The results of this model have been compared with those obtained with the PAMD model from Refs. [9,25], also diagonalized in the THO basis. In this case, $0 \leq \ell \leq 3$ and $1 \leq n \leq 30$ are used. This model only considers the ground state 0^+ and the first-excited state 2^+ for the core, so it would not be consistent to consider higher values of ℓ .

A. Structure of ^{17}C

In the Nilsson calculations presented in this work, the geometry of the central Woods-Saxon potential used in Ref. [5] for ^{17}C is adopted ($R = 3.266$ fm, $a = 0.67$ fm). The strength of this central potential $V_c(r)$ is fixed to 44.27 MeV. Consequently, following the relation from Ref. [16], a 8.825 MeV strength is obtained for the spin-orbit part $V_{\ell s}(r)$ keeping the same geometry. The value $\hbar/2\mathcal{J} = 0.3$ MeV is used for the core Hamiltonian, compatible with the excitation energy of the first-excited state 2^+ of ^{16}C (1.766 MeV [27]). The deformation parameter β takes the value 0.34, similar to the value 0.33 used by Amos *et al.* [28]. The deformation obtained in the Nilsson model can be compared with the PAMD calculation following the prescription of Ref. [8] and considering as radius of the core the inflection point of the central potential. For ^{17}C , we obtain $\beta = 0.44$, 29% larger than the value obtained in the Nilsson model.

With these parameters, the Hamiltonian is fully defined and diagonalized in the THO basis using $b = 2.4$ fm and $\gamma = 2.7$ fm $^{1/2}$. Thus, the energies of the bound states of ^{17}C , shown in the central spectrum of Fig. 2, are negative eigenvalues of this Hamiltonian. In the same figure, on the left, the experimental values [29,30] for these levels are shown and, on the right, the results of the PAMD model. In all cases we have a $3/2^+$ ground state, a $1/2^+$ first excited and a $5/2^+$ second-excited state. It should be noted that while the PAMD model predicts the second-excited state as a near-threshold resonance, in the new Nilsson model it appears as a bound state whose energy is closer to the experimental one. Also,

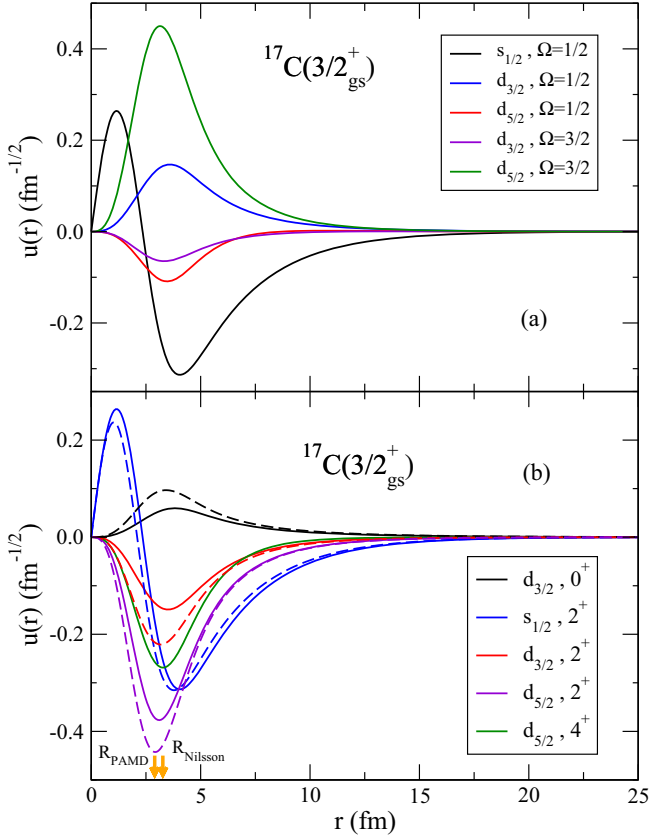


FIG. 3. Radial parts of the wave function obtained for the ground state of ^{17}C . The panel (a) shows the most relevant components in the Nilsson model according to their quantum numbers ℓ , j , and Ω . The panel (b) shows the components, both for the Nilsson (solid lines) and PAMD (dashed lines) models, according to ℓ , j , and I . Core radius for these two models are indicated with arrows.

the first-excited state is closer in energy to the experimental value in the Nilsson model than in the PAMD.

To assess possible improvements of the PAMD model, some particle-rotor models adjusted to the geometry obtained with the PAMD model have been tested. From the analysis of these results, it is obtained that including the 4^+ state of ^{16}C is needed to significantly improve the spectrum, considering in this case states of ^{16}C up to $\ell = 4$. The need to include the 4^+ state for a better description of the ^{17}C spectrum is also suggested in Ref. [28]. Thus, a possible improvement of the PAMD model would be to include this 4^+ state that would require extra transition densities. Other changes, such as a more suitable spin-orbit potential, would be useful, but by themselves they do not achieve the required spectrum agreement.

The radial parts of the ground-state wave function are shown in Fig. 3. The top panel shows the functions $u_\nu(r) = rR_{\varepsilon\nu}^{J^\pi}(r)$ for the Nilsson model, whereas on the lower panel the functions $u_\alpha(r) = rR_{\varepsilon\alpha}^{J^\pi}(r)$ are compared for both models. It is also shown the radius of the core for both models, R_{PAMD} and R_{Nilsson} , obtained as the inflection point of the corresponding central potential. The resulting functions differ mainly in the norm of the components, which are the weights of Table I.

TABLE I. Weights of the main components for the wave function of the ground state and first-excited state of ^{17}C . Components with weights less than 0.005 are not included.

State	$3/2_{\text{gs}}^+$		$1/2_1^+$	
	Nilsson	PAMD	Nilsson	PAMD
$ (\ell s)j \otimes 0^+\rangle$	0.012	0.028	0.668	0.512
$ s_{1/2} \otimes 2^+\rangle$	0.375	0.349		
$ d_{3/2} \otimes 2^+\rangle$	0.064	0.131	0.028	0.040
$ d_{5/2} \otimes 2^+\rangle$	0.366	0.492	0.299	0.448
$ d_{5/2} \otimes 4^+\rangle$	0.179			

In our assumed simplified two-body model, in which antisymmetrization between the valence neutron and the core is neglected, spectroscopy factors (SF) cannot be strictly obtained. However, as long as these antisymmetrization effects are not large, these weights can be approximately regarded as SF. It should be noted that the Nilsson model predicts a non-negligible weight for the component with a 4^+ core state, while the PAMD model does not consider this core state. This means that, in general, the rest of the weights are lower in the Nilsson model.

Figure 4 shows the radial parts of the first-excited state wave function of ^{17}C . It can be seen that the spatial extension is much larger in this case. The root mean square radius for this state is 6.55 fm in the Nilsson model and 5.24 fm in the PAMD, while for the ground state the value is around 4 fm in both models. Therefore, the results of both models corroborate the halo nature of this state. Table I also compares the weights of the components for this state.

The differences here are slightly affected by the energy discrepancy between PAMD and experimental spectra. However, as shown in Ref. [9], the wave functions vary very little if one readjusts the interaction to put the state at the right energy besides the obvious change on the asymptotic decay. Weights relevant for present transfer calculations, for example, remain

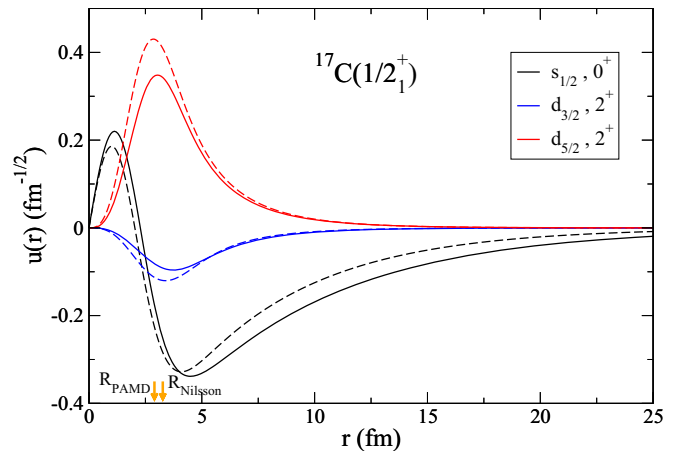


FIG. 4. Radial part of the wave function obtained for the first-excited state of ^{17}C . The results of the Nilsson (solid lines) and PAMD (dashed lines) models are compared, the arrows indicate the core radius for each model.

basically unchanged with a variation of up to 3%. Therefore, this will not influence significantly transfer cross section results included in Sec. V. For s waves, one should also consider that the radial distribution will change if one approaches the $^{16}\text{C}(0^+) + n$ threshold. In Ref. [9], one can see that by setting the bound state $1/2^+$ to the experimental energy, the root mean square radius increases by 10%, approaching the value obtained in the Nilsson model.

B. Structure of ^{11}Be

The ^{11}Be nucleus has been extensively studied in previous works which successfully reproduce structure observables. Our Nilsson Hamiltonian for ^{11}Be uses as starting point the model Be12-b of Ref. [31], which consists of a Woods-Saxon central potential with a parity-dependent strength, a spin-orbit potential with strength 8.5 MeV (both with $R = 2.483$ fm, $a = 0.65$ fm) and a permanent quadrupole deformation with $\beta = 0.67$. This value is consistent with the value $\beta = 0.7$ extracted from the PAMD model following the prescription of Ref. [8] and considering the inflection point of the central potential as R . Our Nilsson model also uses $\hbar/2\mathcal{J} = 0.56$ MeV for the ^{10}Be core, which is compatible with the excitation energy of its first 2^+ state (3.368 MeV [32]). With the rest of the parameters already set, the parity-dependent strength is adjusted slightly to reproduce the experimental energies of the bound states (52.43 MeV for positive-parity states and 49.62 MeV for negative ones). In the same way, the PAMD model allows for a parity-dependent renormalization factor. The purpose of this parity dependence is to reproduce the inversion of the $1/2^+$ and $1/2^-$ bound-state levels of ^{11}Be . As explained in Ref. [8], this inversion is partly ascribed to core deformation, but also to other effects not included in our treatment. In any case, the difference between strengths according to parity does not exceed 6% for both models.

The Nilsson Hamiltonian is diagonalized in a THO basis with $b = 2.0$ and $\gamma = 2.5$ fm $^{1/2}$. Figure 5 compares the ^{11}Be states obtained with this model up to 4 MeV, those obtained with PAMD and the experimental levels [33,34]. In this figure, in addition to the $^{10}\text{Be}(0^+) + n$ threshold, the $^{10}\text{Be}(2^+) + n$ threshold is also indicated. Both models reproduce the experimental energies of the ground state $1/2^+$ and the first-excited state $1/2^-$, while the energies of the resonances $5/2^+$, $3/2^-$, and $3/2^+$ are better reproduced in the PAMD model. In case of the $5/2^-$ resonance, the Nilsson model predicts it above 4 MeV and, for the PAMD model, it is well below. The reason for this difference is the effect of including the 4^+ core state in the calculation. In the PAMD model, the state $5/2^-$ corresponds mostly to a $|p_{1/2} \otimes 2^+\rangle$ configuration. However, in the Nilsson model, there is a mixture of configurations $|p_{3/2} \otimes 4^+\rangle$ and $|p_{1/2} \otimes 2^+\rangle$ resulting in two possible $5/2^-$ resonances. One of them, for which the component with $p_{3/2}$ dominates, is close to the threshold $^{10}\text{Be}(0^+) + n$, but it is a forbidden state due to the Pauli exclusion principle. The other is allowed, but it is above 4 MeV.

Figure 6 compares the wave function of the ^{11}Be ground state obtained for the Nilsson (the most relevant components) and PAMD models. The results are quite similar, with a clear dominance of the $|s_{1/2} \otimes 0^+\rangle$ component. It can be seen that

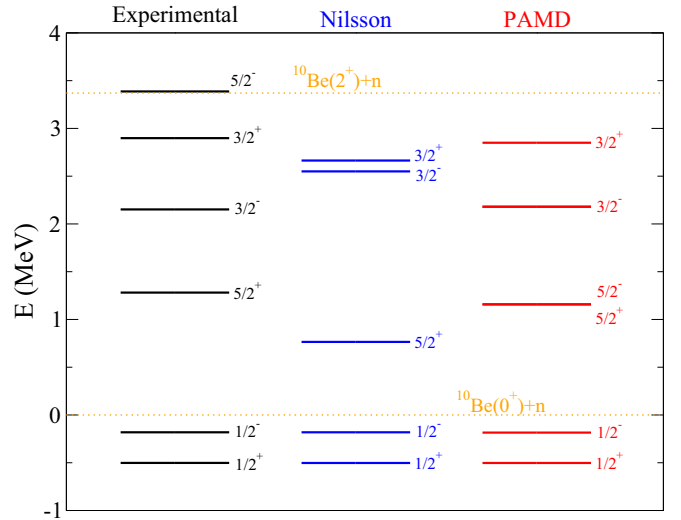


FIG. 5. Spectrum obtained for ^{11}Be with the Nilsson and the PAMD models calculations compared with the experimental one [33,34].

this component has a greater weight in the PAMD model, while the opposite occurs with the $|d_{5/2} \otimes 2^+\rangle$ component. Clearly, the $|d_{3/2} \otimes 2^+\rangle$ component is not very relevant for this state. Likewise, Fig. 7 shows the radial part of the wave function for the first $5/2^+$ resonance obtained in both models. Since the resonances occur at different energies depending on the model, the asymptotic part is clearly different. However, the behavior is very similar for $r < 5$ fm.

V. APPLICATION TO REACTIONS

The differential cross sections for the transfer reactions $^{16}\text{C}(d, p)^{17}\text{C}$ and $^{11}\text{Be}(p, d)^{10}\text{Be}$ have been calculated using the adiabatic distorted-wave approximation (ADWA) [11]. The *post* and the *prior* forms are used, respectively, which require the overlap functions $\langle ^{17}\text{C} | ^{16}\text{C} \rangle$ and $\langle ^{10}\text{Be} | ^{11}\text{Be} \rangle$.

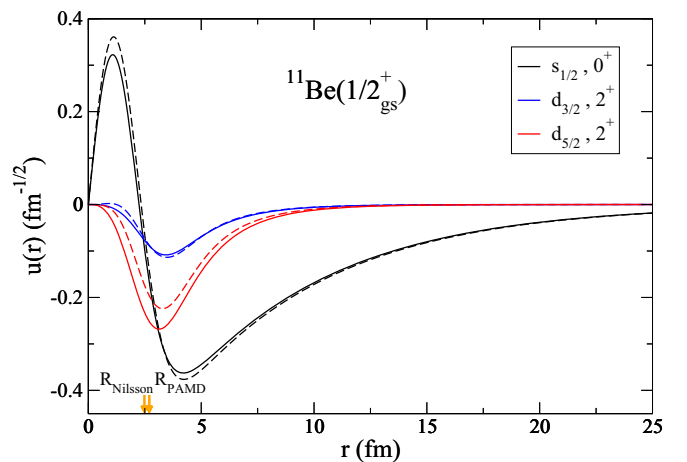


FIG. 6. Radial parts of the ground-state wave function of ^{11}Be . Solid and dashed lines correspond, respectively, to the Nilsson and PAMD models. Core radii are marked with arrows.

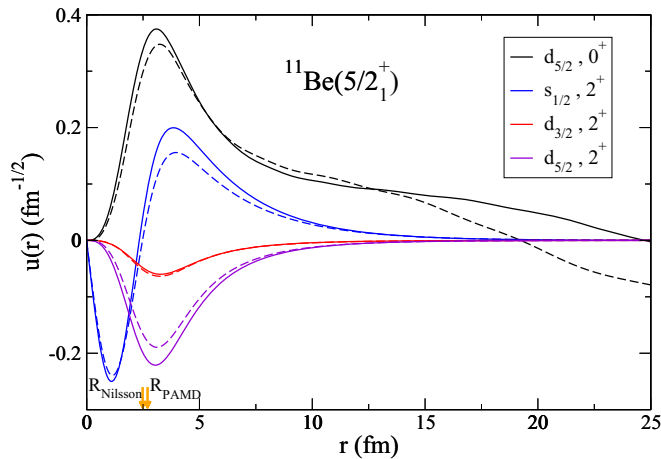


FIG. 7. Radial parts of the continuum wave function for the first ^{11}Be resonance. The Nilsson wave function (solid lines) corresponds to an energy of 0.77 MeV above the $^{10}\text{Be}(0^+) + n$ threshold, while the result of the PAMD model (dashed lines) is for 1.14 MeV. For both models the core radius is indicated with an arrow.

These functions are taken from the results of our structure models.

A. $^{16}\text{C}(d, p)^{17}\text{C}$

For this reaction, the cross section for the transfer to bound states of ^{17}C has been calculated. The results are compared with the recent experimental data from GANIL [10]. These data were obtained in inverse kinematics with a ^{16}C beam at 17.2 MeV/nucleon. Regarding the potentials used in the reaction calculation, the Chapel-Hill (CH89) parametrization [35] was employed for the $p + ^{17}\text{C}$ optical potential, whereas the Reid soft-core potential [36] was used for the $n + p$ interaction. The $d + ^{16}\text{C}$ adiabatic potential was built within the Johnson-Tandy finite-range prescription [37], assuming the CH89 parametrization for the nucleon + ^{16}C potentials.

Figure 8 shows the comparison of the results of the two models with the experimental data when the first- and second-excited states of ^{17}C are populated. For the case of the first-excited state, we find good agreement between the results of our models and the data [Fig. 8(a)]. From the comparison of the experimental data with finite-range ADWA calculations using the CH89 parametrization, spectroscopy factors (SF) are obtained in Ref. [10]. A value of 0.80 ± 0.22 was extracted for the configuration $|s_{1/2} \otimes 0^+\rangle$ of the ^{17}C $1/2_1^+$ state. This SF is compatible with the value 0.67 obtained with the Nilsson model, but not so much with the 0.51 of the PAMD (see Table I). For the second-excited state [Fig. 8(b)], both models provide a reasonable agreement for the angular distribution, although they underestimate the experimental cross section. From these data, a 0.62 ± 0.13 spectroscopy factor is obtained for the configuration $|d_{5/2} \otimes 0^+\rangle$, while the Nilsson and PAMD models predict smaller values, namely, 0.33 and 0.32, respectively. To improve the agreement with the data, it would be necessary for our structure model to obtain a larger weight of this $|d_{5/2} \otimes 0^+\rangle$ component. For that, a more accurate

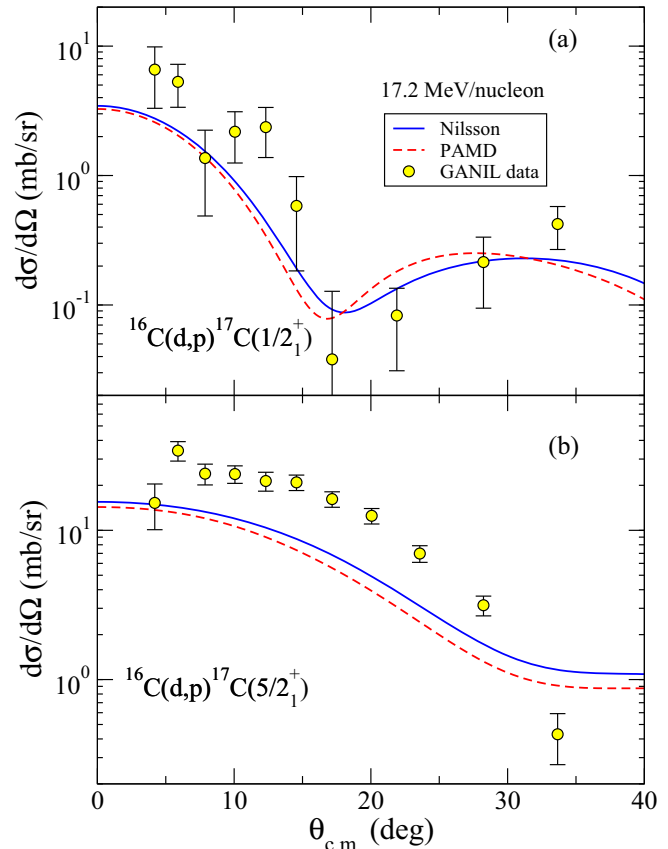


FIG. 8. Angular distribution of the $^{16}\text{C}(d, p)^{17}\text{C}$ reaction at 17.2 MeV/nucleon when the ^{17}C first-excited state $1/2_1^+$ (a), and second-excited state $5/2_1^+$ (b) are populated. The results using the Nilsson and PAMD models are compared with the experimental data [10].

treatment of the Pauli exclusion principle and antisymmetrization would be possibly needed.

To distinguish these two states experimentally it was necessary to measure γ rays in coincidence and hence the angular distribution for the ground state is not presented. However, Fig. 9 shows the angular distribution when any of the bound states of ^{17}C are populated; that is, the sum of contributions from all these states. Furthermore, the analysis of the transfer data performed in Ref. [10] predicts for the $|d_{3/2} \otimes 0^+\rangle$ configuration a very small spectroscopic factor, below 0.08, in agreement with the prediction of the two models considered here (cf. Table I). Considering the results, transfer to the second-excited state $5/2^+$ is by far the greatest contribution for this reaction; therefore, the discrepancy between the data and our calculations comes mainly from the one we found for this state.

B. $^{11}\text{Be}(p, d)^{10}\text{Be}$

The differential cross section for this transfer reaction has been calculated when the ground state 0^+ and first-excited state 2^+ of ^{10}Be are populated. Calculations have been performed for two different incident energies and the results are compared with the experimental data corresponding to those energies. For both energies, the calculations have been

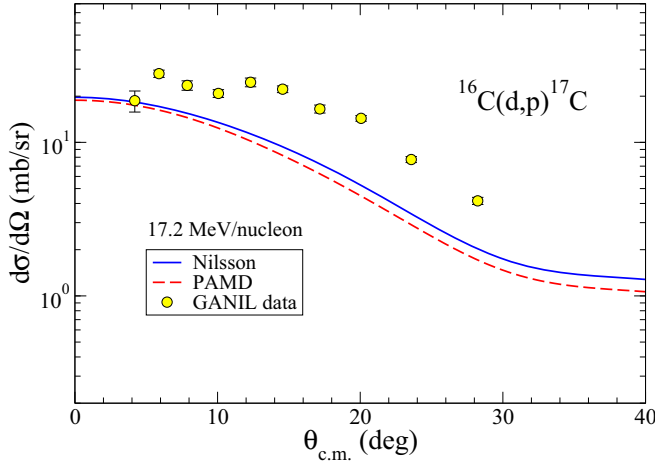


FIG. 9. Differential cross section of $^{16}\text{C}(d, p)^{17}\text{C}$ for transfer to all bound states at 17.2 MeV/nucleon. For both models, the sum of the results for all bound states are shown and they are compared with the experimental data [10].

performed using the Johnson-Tandy prescription for the $d + ^{10}\text{Be}$ potential [37] and the Reid Soft-Core $n + p$ interaction [36]. Experimentally, in both cases the reaction has been studied in inverse kinematics using a ^{11}Be beam.

First, the comparison of our calculations with the data from the Research Center for Nuclear Physics (RCNP) for a ^{11}Be beam 26.9 MeV/nucleon [38] is shown in Fig. 10. For this calculation, a renormalized CH89 parametrization has been used for the $p + ^{11}\text{Be}$ optical potential [39]. This potential applies two normalization factors to the central part of the CH89 parametrization to improve the agreement with the experimental data of the elastic scattering at 26.9 MeV/nucleon: 0.78 for the real part and 1.02 for the imaginary part. CH89 parametrization was also employed for the construction of the $d + ^{10}\text{Be}$ adiabatic potential.

Taking into account the error bars in Fig. 10, the results of both models are compatible with the experimental data. Figure 10(a) corresponds to the transfer to the ground state of ^{10}Be (0^+), where the results of both models are remarkably similar. However, Fig. 10(b) shows that, when the first-excited state 2^+ is populated, the PAMD model gives a smaller cross section, getting closer to the data.

GANIL data for a beam at 35.3 MeV/nucleon [40] are compared with our results in Fig. 11. In this case, for the calculations, the $p + ^{11}\text{Be}$ potential was obtained from the parametrization of Watson, Sigh, and Segel [41]. For consistency, the same parametrization is used for the construction of the adiabatic $d + ^{10}\text{Be}$ potential.

Both models provide reasonable overall agreement with the experimental data. The Nilsson model is slightly closer to the data for the transfer leading to the ^{10}Be ground state [Fig. 11(a)]. However, Fig. 11(b) shows how the PAMD model is again the closest to the data for the transfer to the 2^+ state of ^{10}Be .

In Refs. [38] and [40], some values of spectroscopic factors (SFs) for the $\langle ^{10}\text{Be} | ^{11}\text{Be} \rangle$ overlap were obtained from the comparison of the measured data with ADWA calcula-

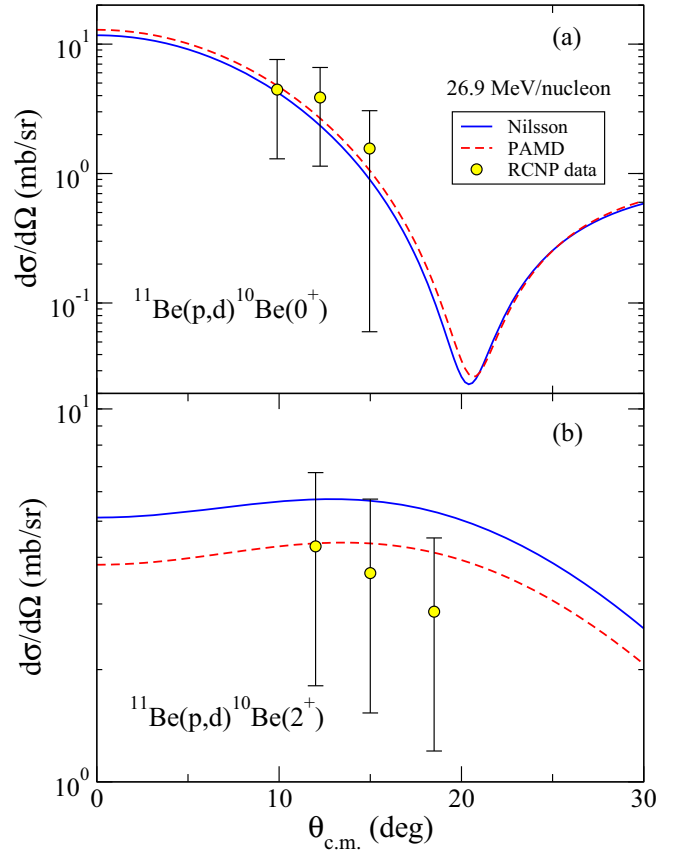


FIG. 10. Angular distribution of the $^{11}\text{Be}(p, d)^{10}\text{Be}$ cross section at 26.9 MeV/nucleon when ^{10}Be ground state 0^+ (a), and first-excited state 2^+ (b) are populated. The solid lines represent the results applying the different models and they are compared with the experimental data [38].

tions. As the weights of the α components are considered an approximation of these spectroscopic factors, in Table II, the experimental SF are compared with the weights obtained through the Nilsson and PAMD models. In general, the weights of both models are approximately compatible with the ranges of experimental values for SF. Note that there is a significant difference between the Nilsson and PAMD models in the case of $\langle ^{10}\text{Be}(2^+) | ^{11}\text{Be}(1/2_{gs}^+) \rangle$ overlap, due to the aforementioned difference in the component $|d_{5/2} \otimes 2^+\rangle$. This is the main reason for the discrepancy between the models for the $^{11}\text{Be}(p, d)^{10}\text{Be}(2^+)$ differential cross section.

TABLE II. Spectroscopic factors for the $^{11}\text{Be}(p, d)^{10}\text{Be}$ reaction to the 0^+ ground state and 2^+ excited state in ^{10}Be . The values resulting from our theoretical models are compared with the ranges of values from the analysis of the experimental data.

SF	Experimental data		Theoretical model	
	RCNP [38]	GANIL [40]	Nilsson	PAMD
$ ^{11}\text{Be}(1/2_{gs}^+)\rangle$				
$\langle ^{10}\text{Be}(0^+) $	0.82 ± 0.15	0.66–0.80	0.78	0.85
$\langle ^{10}\text{Be}(2^+) $	0.26 ± 0.09	0.13–0.38	0.21	0.15

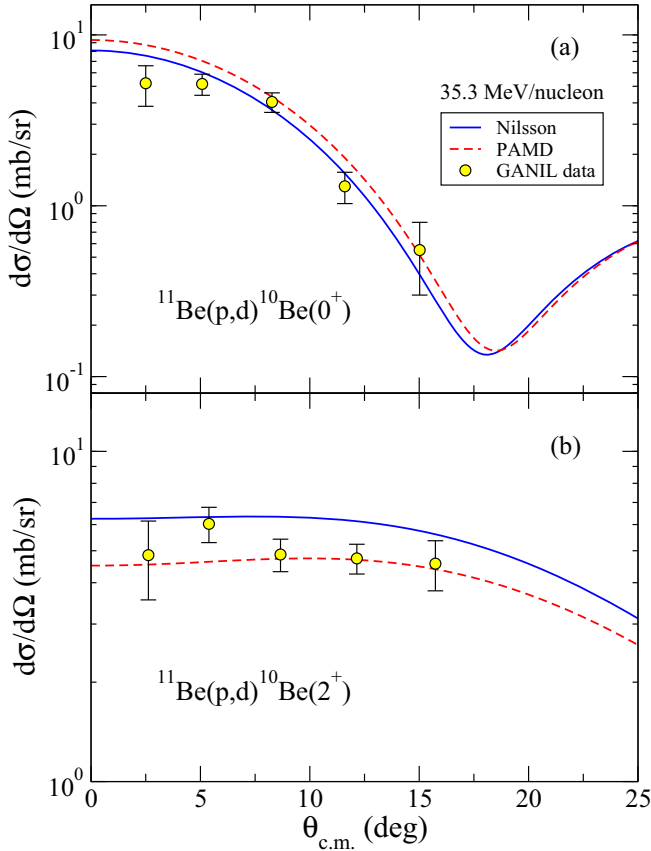


FIG. 11. Differential cross section for the $^{11}\text{Be}(p,d)^{10}\text{Be}$ transfer reaction to $^{10}\text{Be}(0^+)$ (a) and $^{10}\text{Be}(2^+)$ (b). The calculations for 35.3 MeV/nucleon are compared with the experimental data from GANIL [40].

VI. SUMMARY AND CONCLUSIONS

A deformed two-body approach based on the Nilsson model has been applied to the study of exotic nuclei, with emphasis on one-neutron halo nuclei. This model considers a neutron moving in a deformed potential generated by the core. This interaction consists of central Woods-Saxon potential, a noncentral term that assumes the permanent axial quadrupole deformation of the former and a spin-orbit term. The full Hamiltonian of the system also includes a collective rotational term to account for core excitation. The results of this model are compared with those of the PAMD model [8]. In both cases the energies and wave functions are obtained by diagonalizing the Hamiltonian in the transformed harmonic oscillator (THO) basis. Using the adiabatic distorted-wave approximation (ADWA), the results of our two models have been applied to the study of one-neutron transfer reactions and their application to break up reactions is in progress.

The Nilsson and PAMD models have been applied to ^{17}C , whose first-excited state is a one-neutron halo candidate, and to the well-known halo nucleus ^{11}Be . Using the deformation parameter $\beta = 0.34$, the Nilsson model gives a good description of the bound states in ^{17}C , better than the semimicroscopic PAMD model. From the analysis of the results, the relevance of the 4^+ core state stands out, a state that is

not included in the PAMD model. Furthermore, both models present a large spatial extension in the wave function of the first-excited state, supporting the halo nature of this state. On the other hand, the PAMD model better reproduces the experimental spectrum of ^{11}Be . However, the Nilsson model predicts similar results by applying a deformation of $\beta = 0.67$. In both models, a parity-dependent strength is needed, but the difference between parities is less than 6%.

The structure models are tested by studying the transfer reactions $^{16}\text{C}(d,p)^{17}\text{C}$ and $^{11}\text{Be}(p,d)^{10}\text{Be}$. For the former, calculations were performed for an energy of 17.2 MeV/nucleon, and the results were compared with the experimental data from GANIL [10]. Good agreement is found with the data for the differential cross section for to the ^{17}C first-excited state ($1/2_1^+$). As discussed in Ref. [10], this state is a candidate for being a halo state. Both models predict a large extension for this state and provide a good reproduction of the experimental data, thus adding more evidence to the halo nature of this excited state. In case of the second-excited state $5/2_1^+$, our calculations are clearly below the experimental data. This suggests that the weight of the component $|d_{5/2} \otimes 0^+\rangle$ of the $5/2_1^+$ state, should probably be higher than the values obtained with the two models presented here. In general, although the results of both models are very similar, we can conclude that the Nilsson model are closer to the data. This work shows the transfer to the bound states of ^{17}C , but the transfer to the continuum states is also being studied and the results will be presented in a subsequent publication.

The $^{11}\text{Be}(p,d)^{10}\text{Be}$ transfer reaction has been studied at two different energies, 26.9 MeV/nucleon and 35.3 MeV/nucleon. In the first case, the results of the reaction calculations using the two different structure models are compared with the RCNP data [38] and, in the other case, the calculations are compared with the experimental data from GANIL [40]. In both cases, for the transfer to the ground state of ^{10}Be , a reasonable agreement is obtained with the two models. For the transfer to the first-excited state of ^{10}Be , the PAMD model is closer to the data. This is mainly due to the fact that the weight of the $|d_{5/2} \otimes 2^+\rangle$ component is smaller in this model.

Since the PAMD model provides better results both in the transfer cross section and for the predicted resonant energies, this model seems to be more adequate to describe the structure of ^{11}Be . However, for ^{17}C , the Nilsson model gives a more accurate description of both the spectrum and the transfer reaction studied, making it a more suitable framework for modeling the structure of ^{17}C . This may be due to the inclusion of the 4^+ core state by the Nilsson model, which is absent in our PAMD model. In view of these results, it would be interesting to extend the PAMD model presented here by including, at least, the 4^+ excited state of the core. This would require the knowledge of the corresponding transition densities which, in principle, could be also evaluated within the AMD model. The importance of including this ^{16}C state has been suggested by other models [28]. It can also be an indication of how, depending on the nucleus, the strong- or weak-coupling approach between the valence nucleon and core is more appropriate. In any case, both deformed two-body models reasonably described the structure

of ^{17}C and ^{11}Be . Furthermore, because they use the same THO formalism, they can be equally easily used in reactions calculations.

A pending task for these two models is a more correct application of the Pauli principle. Here we have removed those final bound eigenstates that we consider occupied by comparing with the spherical and Nilsson limits. The Nilsson model is more convenient in this regard because it allows single-particle Nilsson states to be removed or partially blocked in a more sophisticated way.

The Nilsson-inspired model presented here and the PAMD model have been applied for the first time to transfer reactions with ^{17}C and ^{11}Be . Application to ^{19}C is in progress and extension to other weakly bound nuclei is planned. As both models also provide radial wave functions, the halo nature of the nuclei will be consistently considered in the analysis of the

reaction. In addition, it is intended to incorporate microscopic information into the model, in a way similar to what is done in the PAMD model or even beyond.

ACKNOWLEDGMENTS

The present research is funded from Grant No. PID2020-114687GB-I00 by MCIN/AEI/10.13039/501100011033, the project PAIDI 2020 with Ref. P20_01247 by the Consejería de Transformación Económica, Industria, Conocimiento y Universidades, Junta de Andalucía (Spain), and by ERDF A way of making Europe. P.P. acknowledges Ph.D. grants from the Ministerio de Universidades and the Consejería de Transformación Económica, Industria, Conocimiento y Universidades, Junta de Andalucía.

-
- [1] A. M. Moro and R. Crespo, Core excitation effects in the breakup of the one-neutron halo nucleus ^{11}Be on a proton target, *Phys. Rev. C* **85**, 054613 (2012).
- [2] A. M. Moro and J. A. Lay, Interplay Between Valence and Core Excitation Mechanisms in the Breakup of Halo Nuclei, *Phys. Rev. Lett.* **109**, 232502 (2012).
- [3] A. Deluva, Faddeev-type calculation of three-body nuclear reactions including core excitation, *Phys. Rev. C* **88**, 011601(R) (2013).
- [4] J. A. Lay, R. de Diego, R. Crespo, A. M. Moro, J. M. Arias, and R. C. Johnson, Evidence of strong dynamic core excitation in ^{19}C resonant break-up, *Phys. Rev. C* **94**, 021602(R) (2016).
- [5] I. Hamamoto, Nilsson diagrams for light neutron-rich nuclei with weakly-bound neutrons, *Phys. Rev. C* **76**, 054319 (2007).
- [6] I. Hamamoto and S. Shimoura, Properties of ^{12}Be and ^{11}Be in terms of single-particle motion in deformed potential, *J. Phys. G* **34**, 2715 (2007).
- [7] J. Casal, E. Garrido, R. de Diego, J. M. Arias, and M. Rodríguez-Gallardo, Radiative capture reaction for ^{17}Ne formation within a full three-body model, *Phys. Rev. C* **94**, 054622 (2016).
- [8] J. A. Lay, A. M. Moro, J. M. Arias, and Y. Kanada-En'yo, Semi-microscopic folding model for the description of two-body halo nuclei, *Phys. Rev. C* **89**, 014333 (2014).
- [9] P. Punta, J. A. Lay, and A. M. Moro, The role of deformation in the ^{17}C structure and its influence in transfer and breakup reactions, EPJ Web Conf. (to be published).
- [10] X. Pereira-López, B. Fernández-Domínguez, F. Delaunay, N. Achouri, N. Orr, W. Catford, M. Assié, S. Bailey, B. Bastin, Y. Blumenfeld, R. Borcea, M. Caamaño, L. Caceres, E. Clément, A. Corsi, N. Curtis, Q. Deshayes, F. Farget, M. Fischella, G. de France *et al.*, Low-lying single-particle structure of ^{17}C and the $N = 14$ sub-shell closure, *Phys. Lett. B* **811**, 135939 (2020).
- [11] R. C. Johnson and P. J. R. Soper, Contribution of deuteron breakup channels to deuteron stripping and elastic scattering, *Phys. Rev. C* **1**, 976 (1970).
- [12] A. O. Macchiavelli, H. L. Crawford, C. M. Campbell, R. M. Clark, M. Cromaz, P. Fallon, M. D. Jones, I. Y. Lee, A. L. Richard, and M. Salathe, Spectroscopic factors in the $N = 20$ island of inversion: The Nilsson strong-coupling limit, *Phys. Rev. C* **96**, 054302 (2017).
- [13] A. O. Macchiavelli, H. L. Crawford, C. M. Campbell, R. M. Clark, M. Cromaz, P. Fallon, M. D. Jones, I. Y. Lee, and M. Salathe, Analysis of spectroscopic factors in ^{11}Be and ^{12}Be in the Nilsson strong-coupling limit, *Phys. Rev. C* **97**, 011302(R) (2018).
- [14] A. O. Macchiavelli, H. L. Crawford, C. M. Campbell, R. M. Clark, M. Cromaz, P. Fallon, M. D. Jones, I. Y. Lee, and M. Salathe, Erratum: Analysis of spectroscopic factors in ^{11}Be and ^{12}Be in the Nilsson strong-coupling limit *Phys. Rev. C* **97**, 011302(R) (2018), *Phys. Rev. C* **97**, 049902(E) (2018).
- [15] A. Broad, D. Lewis, W. Gray, P. Ellis, and A. Dudek-Ellis, Inelastic processes and form factor effects in the $^{162,164}\text{Dy}(^3\text{He}, d)$ reactions at 46.5 MeV, *Nucl. Phys. A* **273**, 69 (1976).
- [16] I. Hamamoto, One-particle resonant levels in a deformed potential, *Phys. Rev. C* **72**, 024301 (2005).
- [17] Y. Kanada-En'yo, H. Horiuchi, and A. Ono, Structure of Li and Be isotopes studied with antisymmetrized molecular dynamics, *Phys. Rev. C* **52**, 628 (1995).
- [18] Y. Kanada-En'yo, F. Kobayashi, and T. Suhara, Structures of ground and excited states in C isotopes, *J. Phys.: Conf. Ser.* **445**, 012037 (2013).
- [19] D. M. Brink and G. R. Satchler, *Angular Momentum* (Clarendon, Oxford, 1968).
- [20] A. Bohr and B. Mottelson, in *Nuclear Structure*, edited by W. A. Benjamin (World Scientific Publishing Company, New York, 1969).
- [21] M. V. Stoitsov and I. Z. Petkov, Density functional theory at finite temperatures, *Ann. Phys. (NY)* **184**, 121 (1988).
- [22] I. Z. Petkov and M. V. Stoitsov, Density functional theory at finite temperatures, *Nuclear Density Functional Theory, Oxford Studies in Physics* (Clarendon, Oxford, 1991).
- [23] S. Karataglidis, K. Amos, and B. G. Giraud, Local scale transformations and extended matter distributions in nuclei, *Phys. Rev. C* **71**, 064601 (2005).
- [24] A. M. Moro, J. M. Arias, J. Gómez-Camacho, and F. Pérez-Bernal, Analytical transformed harmonic oscillator basis for cdcc calculations, *Phys. Rev. C* **80**, 054605 (2009).

- [25] J. A. Lay, A. M. Moro, J. M. Arias, and J. Gómez-Camacho, Particle motion in a deformed potential using a transformed oscillator basis, *Phys. Rev. C* **85**, 054618 (2012).
- [26] I. Thompson, Coupled reaction channels calculations in nuclear physics, *Comput. Phys. Rep.* **7**, 167 (1988).
- [27] D. Tilley, H. Weller, and C. Cheves, Energy levels of light nuclei $A = 16$ – 17 , *Nucl. Phys. A* **564**, 1 (1993).
- [28] K. Amos, L. Canton, P. Fraser, S. Karataglidis, J. Svenne, and D. van der Knijff, Linking the exotic structure of ^{17}C to its unbound mirror ^{17}Na , *Nucl. Phys. A* **879**, 132 (2012).
- [29] W. Meng, G. Audi, F. G. Kondev, and S. Naimi, The AME2016 atomic mass evaluation (II). Tables, graphs and references, *Chin. Phys. C* **41**, 030003 (2017).
- [30] Z. Elekes, Z. Dombrádi, R. Kanungo, H. Baba, Z. Fülöp, J. Gibelin, Á. Horváth, E. Ideguchi, Y. Ichikawa, N. Iwasa, H. Iwasaki, S. Kanno, S. Kawai, Y. Kondo, T. Motobayashi, M. Notani, T. Ohnishi, A. Ozawa, H. Sakurai, S. Shimoura *et al.*, Low-lying excited states in $^{17,19}\text{C}$, *Phys. Lett. B* **614**, 174 (2005).
- [31] F. Nunes, J. Christley, I. Thompson, R. Johnson, and V. Efros, Core excitation in three-body systems: Application to ^{12}Be , *Nucl. Phys. A* **609**, 43 (1996).
- [32] D. Tilley, J. Kelley, J. Godwin, D. Millener, J. Purcell, C. Sheu, and H. Weller, Energy levels of light nuclei $A = 8, 9, 10$, *Nucl. Phys. A* **745**, 155 (2004).
- [33] J. Kelley, E. Kwan, J. Purcell, C. Sheu, and H. Weller, Energy levels of light nuclei $A = 11$, *Nucl. Phys. A* **880**, 88 (2012).
- [34] N. Fukuda, T. Nakamura, N. Aoi, N. Imai, M. Ishihara, T. Kobayashi, H. Iwasaki, T. Kubo, A. Mengoni, M. Notani, H. Otsu, H. Sakurai, S. Shimoura, T. Teranishi, Y. X. Watanabe, and K. Yoneda, Coulomb and nuclear breakup of a halo nucleus ^{11}Be , *Phys. Rev. C* **70**, 054606 (2004).
- [35] R. L. Varner, W. J. Thompson, T. L. McAbbe, E. J. Ludwig, and T. B. Clegg, A global nucleon optical model potential, *Phys. Rep.* **201**, 57 (1991).
- [36] R. V. Reid, Local phenomenological nucleon-nucleon potentials, *Ann. Phys. (NY)* **50**, 411 (1968).
- [37] R. Johnson and P. Tandy, An approximate three-body theory of deuteron stripping, *Nucl. Phys. A* **235**, 56 (1974).
- [38] Y. Jiang, J.-L. Lou, Y.-L. Ye, D.-Y. Pang, J. Chen, Z.-H. Li, Y.-C. Ge, Q.-T. Li, J. Li, W. Jiang, Y.-L. Sun, H.-L. Zang, Y. Zhang, W. Liu, Y.-D. Chen, G. Li, N. Aoi, E. Ideguchi, H. J. Ong, J. Lee *et al.*, A new measurement of $^{11}\text{Be}(p, d)$ transfer reaction, *Chin. Phys. Lett.* **35**, 082501 (2018).
- [39] J. Chen, J. L. Lou, Y. L. Ye, Z. H. Li, Y. C. Ge, Q. T. Li, J. Li, W. Jiang, Y. L. Sun, H. L. Zang, N. Aoi, E. Ideguchi, H. J. Ong, Y. Ayyad, K. Hatanaka, D. T. Tran, T. Yamamoto, M. Tanaka, T. Suzuki, N. T. Tho *et al.*, Elastic scattering and breakup of ^{11}Be on protons at 26.9A MeV, *Phys. Rev. C* **93**, 034623 (2016).
- [40] J. S. Winfield, S. Fortier, W. N. Catford, S. Pita, N. A. Orr, J. Van de Wiele, Y. Blumenfeld, R. Chapman, S. P. G. Chappell, N. M. Clarke, N. Curtis, M. Freer, S. Gales, H. Langevin-Joliot, H. Laurent, I. Lhenry, J. M. Maison, P. Roussel-Chomaz, M. Shawcross, K. Spohr *et al.*, Single-neutron transfer from $^{11}\text{Be}_{\text{gs}}$ via the (p, d) reaction with a radioactive beam, *Nucl. Phys. A* **683**, 48 (2001).
- [41] B. A. Watson, P. P. Singh, and R. E. Segel, Optical-model analysis of nucleon scattering from $1p$ -shell nuclei between 10 and 50 MeV, *Phys. Rev.* **182**, 977 (1969).